FLUORINE-SUPPORTED FLAMES IGNITED BY A PULSED CO_2 LASER

WAYNE M. TROTT

Laser Physical Chemistry Division 1128, Sandia National Laboratories, Albuquerque, NM 87185 (U.S.A.)

Summary

The chemistry accompanying pulsed CO_2 laser irradiation of fuel–SF_6 mixtures was examined using time-integrated visible emission spectroscopy and analysis of the IR absorption spectra of end products. Under suitable conditions of laser energy, gas pressure, mixture ratio and cell geometry, the visible luminescence exhibits characteristics of fluorine-supported flames. Similar emission has been observed in irradiated fuel–S_2F_{10} mixtures. An analysis of ignition delay *versus* absorbed laser energy is presented for CH_4–SF_6 mixtures; it accounts for fluence-dependent absorption by these mixtures and models the effects of hydrodynamic motion on the initial pressure, density and temperature profiles in the samples using a computer code for two-dimensional wave propagation. Many of the IR absorption data are consistent with a reaction mechanism involving the formation of small hydrocarbon intermediates followed by efficient hydrogen abstraction to generate end products such as CS_2, CF_4 and C_2F_4. Mechanisms for reaction initiation are discussed.

1. Introduction

The process of multiple photon excitation and dissociation of polyatomic molecules using intense IR laser radiation has been the subject of extensive experimental investigation and theoretical analysis during the past decade [1 - 6]. Much of this effort has involved SF_6 and related compounds (*e.g.* SF_5Cl and S_2F_{10}). The initiation of chemical reactions using SF_6 as a resonant absorber of pulsed CO_2 laser radiation (in nominally collisional [7 - 9] or non-collisional [10 - 12] excitation regimes) remains an active research area in this regard. Under certain conditions, secondary reactions of SF_6 photofragments with hydrocarbons or other fuel molecules give rise to visible chemiluminescence from electronically excited species such as C_2^* or CH^* [13 - 16] and to chemiluminescence from vibrationally excited HF [17 - 19]. The former phenomenon has been studied in terms of the depen-

dence of luminescence intensity on laser fluence and pressure effects on the delay of onset of emission. The latter result has been exploited in investigations of the multiple-photon dissociation mechanism for SF_6 [17 - 19] as well as in various schemes to produce CO_2-laser-pumped HF lasers [20 - 26].

Qualitative aspects of the chemistry accompanying pulsed CO_2 laser irradiation of a number of different SF_6–fuel and S_2F_{10}–fuel systems (5 - 50 Torr total pressure) are discussed in this paper through analysis of spectral properties of the visible emission and the IR absorption spectra of end products from selected samples. Evidence is presented for CO_2 laser ignition of highly luminous flames from many of these mixtures under appropriate conditions of laser intensity, ratio of SF_6 (or S_2F_{10}) to the fuel and gas confinement. In the case of SF_6-to-CH_4 ratios of 1:1, an approximate quantitative analysis of the ignition delay as a function of temperature (or absorbed laser energy) and initial pressure is given. The data presented do not characterize in detail the chemical kinetics of the various CO_2-laser-initiated reactions; however, the results do indicate the probable complexity of these systems.

2. Experimental details[†]

A detailed discussion of the experimental design has been presented elsewhere [27]. The essential details of this apparatus are illustrated in Fig. 1. Briefly, energy pulses from a grating-tuned Lumonics TEA-103-2 CO_2 laser (the $00^0 1$–$10^0 0$ P(32) line at 10.718 μm) were weakly focused by a mirror with a radius of curvature of 5 m to a cross-sectional area of about 1.6 cm $\times$ 1.6 cm and were directed through one of several test cells. The beam was very nearly collimated over the length of the test region. Transmitted laser energy was measured by an absolutely calibrated absorbing surface disc calorimeter placed behind the cell. A second energy meter monitored a small fraction of the energy incident on the cell. Calibration was maintained between the two detectors. As determined by a pyroelectric detector, the CO_2 laser exhibited the usual temporal behavior, i.e. an initial spike (full width at half-maximum, 100 ns) containing about 50% of the energy followed by an exponentially decaying tail (duration of about 1.5 μs). The spatial profile of the beam incident on the cell was characterized by sampling the energy contained in different regions of the beam using a rectangular aperture of dimensions 1.6 cm $\times$ 0.16 cm. Vertical and horizontal scans indicated the same approximate profile in both directions, i.e.

$$f(x) = \exp\left\{-\left(\frac{x}{a}\right)^4\right\}$$

[†]Reference to a company or product name does not imply exclusive recommendation of the product by the Sandia National Laboratories or the U.S. Department of Energy.
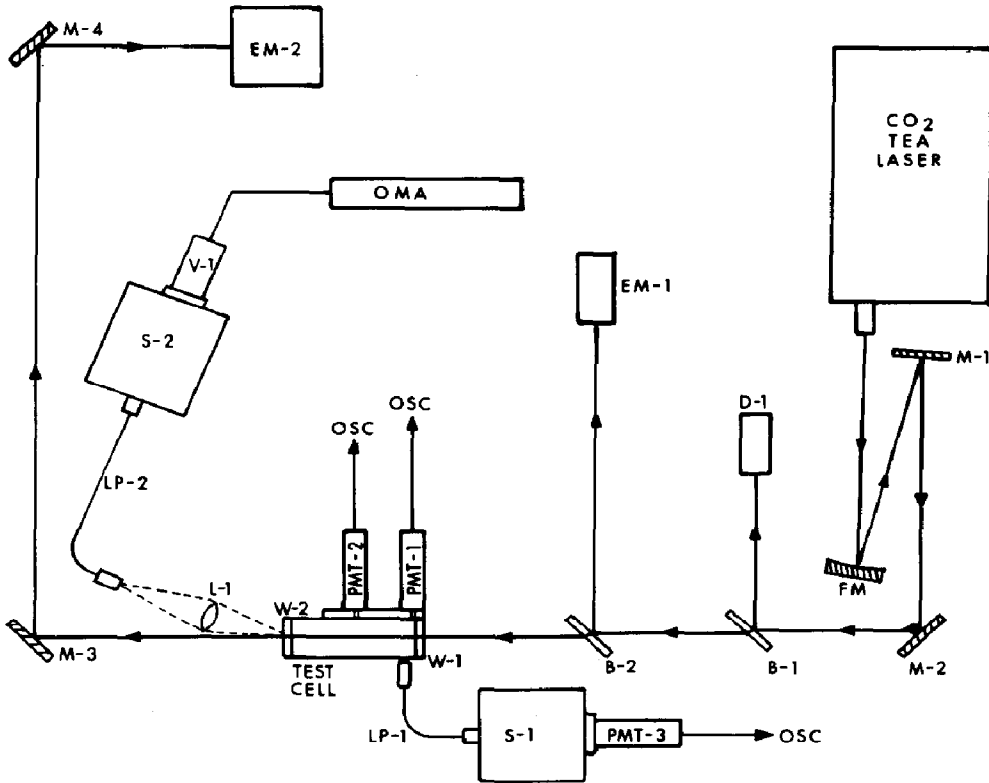
Fig. 1. Schematic diagram of the CO_2 laser ignition test system: M, turning mirrors; FM, focusing mirror; B, beam splitters; W, test cell windows; L, lens; LP, light pipes; PMT, photomultiplier tubes; S, 1/4 m spectrometers; V, Vidicon detector head; OMA, optical multichannel analyzer; EM, energy meters; D, pyroelectric detector. The piezoelectric pressure transducer (mounted on the side of the test cell) and the gas cell for variable-beam attenuation are not shown.

where $x = 0$ refers to the geometric center of the cell opening and a is about 0.65 cm (see ref. 27, Fig. 3). In order to utilize two-dimensional techniques to model energy absorption and hydrodynamic motion in the samples, the observed profile was considered to be equivalent to a cylindrically symmetric beam with radial profile

$$f(r) = \exp\left\{-\left(\frac{r}{a'}\right)^4\right\}$$

For $a' = 0.73$ cm this model profile was capable of reproducing, within a few per cent, the measured transmitted energies through various circular apertures. Incident and exit beam burn patterns indicated no significant problems with either "hot spots" or self-focusing effects in the samples. Variable attenuation of the laser energy was provided by dimethyl ether (0 - 100 Torr) contained in a gas cell 12.5 cm long placed directly in front of the laser. The IR absorption properties of this gas are such that continuous

adjustment of the excitation energy could be effected with negligible changes in the temporal and spatial profile of the beam [27].

The ignition delay measurements and nearly all emission spectra were obtained using a quartz test cell 5 cm long with a square cross-sectional area essentially matching that of the weakly focused laser beam. Polished BaF_2 discs (2.5 cm in diameter and 0.2 cm thick) were used as the entrance and exit windows of this cell. Light emission from an irradiated gas mixture was monitored by two photomultiplier tubes (PMTs), one mounted near the input window and the other near the center of the cell. Each tube was apertured to view a volume of 0.05 cm^3 intersecting the longitudinal axis of the cell. The pressure history in one region of the cell was recorded by a piezoelectric pressure transducer with a rise time of less than 2 μs which was attached to the wall of the cell on an axis perpendicular to the viewing region of the second PMT. Time-integrated emission spectra were obtained by the collection optics and optical multichannel analyzer system shown in Fig. 1. The useful spectral range of this device was 360 - 800 nm and portions of width 40 nm of a given spectrum could easily be observed and recorded on a single shot (see Section 3). Two cylindrical quartz cells were utilized for IR absorption spectral analysis of post-irradiated gas mixtures. The inner diameter and length of the larger cell were 4.4 cm and 9.6 cm respectively. The corresponding dimensions of the smaller cell were 1.6 cm and 4.8 cm respectively. Polished NaCl discs were used for the windows in both cells. The absorption spectra were obtained using a Beckman model 4240 IR spectrophotometer. Copious solid deposits were formed by the laser-initiated reactions. Consequently frequent cell cleaning and window replacement were necessary.

Mixtures containing highly volatile fuels were prepared and thoroughly stirred in an external reservoir. Samples containing low pressure vapor from liquid fuels were prepared by admitting the fuel vapor to the test cell and then adding the SF_6 (or S_2F_{10}) in a turbulent fashion. Gas pressures were determined manometrically. Fuels tested include CH_4, CH_3F, CH_2F_2, CHF_3, NH_3, H_2O, methanol, dimethyl ether, propylene oxide, p-dioxane, nitromethane, n-propyl nitrate, isopropyl nitrate and n-butyl nitrate. All reactants were obtained from commercial suppliers. IR spectral analyses indicated no significant impurities in any of the reactants and no further purification was attempted.

3. Results and discussion

The time-integrated visible emission spectra generated by CO_2-laser-initiated fuel–SF_6 reactions exhibit distinct features which vary dramatically as a function of several experimental parameters including the incident laser energy, gas pressure, ratio of fuel to SF_6 and cell geometry. The variable nature of this emission is illustrated by the two spectra displayed in Fig. 2. Each case represents data taken on a single shot and at identical detector
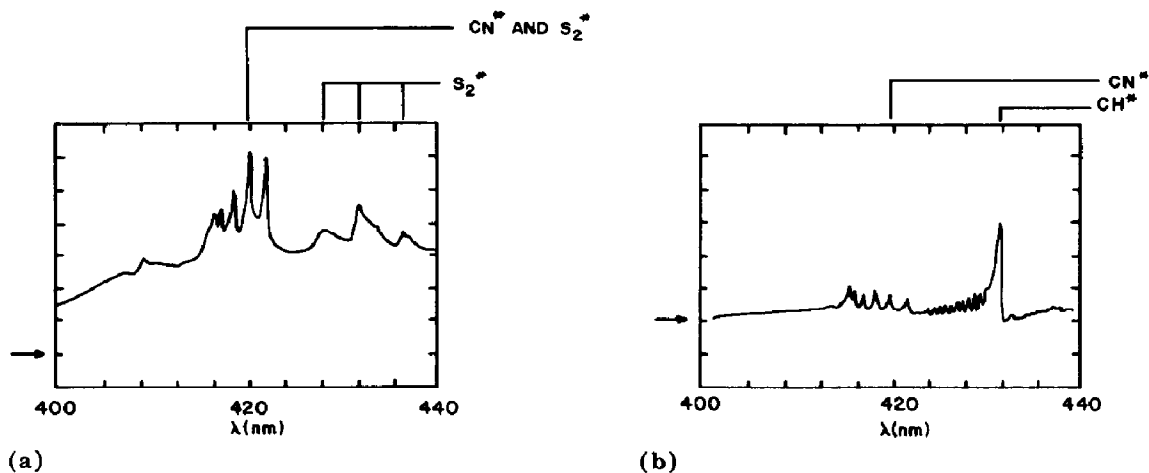
(a)   (b)

Fig. 2. Time-integrated spectra obtained using an optical multichannel analyzer: (a) CO_2-laser-initiated flame from a 1:2 mixture of SF_6 and n-propyl nitrate (20 Torr); (b) chemiluminescence from hydrocarbon impurities (primarily a few tens of millitorrs of n-propyl nitrate) in laser-irradiated SF_6 (11 Torr). In both cases the incident laser energy and maximum (on axis) laser energy fluence were 5.0 J and about 3.5 J cm^{-2} respectively. The arrows indicate zero signal level (background subtracted).

sensitivity. The spectrum shown in Fig. 2(b) was generated under experimental conditions roughly comparable with those reported by other workers [13 - 16]. As indicated, when a small concentration of nitrogen-containing hydrocarbon is irradiated in the presence of an abundance of SF_6 the chemiluminescence observed in the 400 - 440 nm region is dominated by molecular band emission due to CN(B $^2\Sigma$–X $^2\Sigma$) and CH(A $^2\Delta$–X $^2\Pi$). Under the same experimental conditions, the C_2(d $^3\Pi_g$–a $^3\Pi_u$) Swan system is also evident at 468 - 474, 513 - 517 and 550 - 564 nm. The observed duration of the spectrally integrated emission (about 200 μs) is consistent with similar data reported by Orr and Keentok [13]. Very different results may be obtained when mixtures containing higher relative concentrations of fuel are exposed to energetic CO_2 laser pulses. For many fuels, the consequent visible emission exhibits an intense broad band continuum, a relatively long duration (1 - 5 ms) and a delay to emission onset which is dependent on the absorbed energy, *i.e.* characteristics indicating ignition of luminous flames. Typical results for a 20 Torr 1:2 mixture of n-propyl nitrate and SF_6 are illustrated in Fig. 2(a). At constant incident laser energy, similar emission features were observed for this system at fuel-to-SF_6 ratios ranging from 1:3 to 3:1. At ratios below 1:3, the emission characteristics tended toward those displayed in Fig. 2(b), whereas at ratios above 3:1 the absorbed energy was apparently too low to ignite the reaction.

Highly luminous reactions were found to accompany the irradiation of mixtures of fuel and SF_6 in an approximate 1:1 ratio for all fuels tested except NH_3. Although rigorous tests of ease of ignition were not performed, significantly higher absorption (about a factor of 2) was required to ignite mixtures containing dimethyl ether, p-dioxane, H_2O and CHF_3. Irradiation

of 50 Torr NH_3–SF_6 mixtures produced easily discernible but relatively weak and short-lived chemiluminescence even though virtually all the available laser energy (up to 400 mJ cm^{-3} averaged over the entire cell volume of 12.5 cm^3) could be absorbed in this sample. Particularly large amounts of solid deposits were formed in the propylene oxide–SF_6 and dimethyl ether–SF_6 reactions.

In addition to the broad band continuum, interesting molecular band emission occurs in conjunction with the fuel–SF_6 reactions. In general, features corresponding to CN(B $^2\Sigma$–X $^2\Sigma$) emission at 385 - 388 nm and 415 - 422 nm (in the case of nitrogen-containing species) and S_2(B $^3\Sigma_u^-$–X $^3\Sigma_g^-$) emission throughout the visible wavelengths were observed to be predominant, while the usual hydrocarbon combustion features C_2^* and CH* were relatively weak. However, C_2^* bands were seen to be most prominent in the p-dioxane–SF_6 and dimethyl ether–SF_6 flames. Overall, the observed spectra are in accordance with previous observations [28, 29] of molecular- and atomic-fluorine-supported flames, particularly those containing sulfur. Bauer and coworkers [7, 30] have also reported emission from the S_2^* system in conjunction with the CO_2 laser initiation of an explosive reaction between SF_6 and SiH_4.

Although the various fuel–SF_6 flames were temporally self-sustaining, they were observed to remain largely confined to sample volumes experiencing maximum or near-maximum excitation. This phenomenon was evident from the information recorded by the side wall pressure instrumentation (the pressure and temperature elevation readily observed throughout the cell in conjunction with deflagration of fuel–oxygen mixtures [27] was much less obvious in the fuel–SF_6 systems) and was clearly visible when mixtures were excited in the large-diameter cylindrical cell. The substantial heat capacity of SF_6 may play an important role in limiting the spread of the exothermic reactions. Also significant is the coupling of cell geometry and hydrodynamic effects, i.e. in a volume large compared with the excitation region rapid expansion wave cooling takes place on the optical axis after the laser pulse and a relatively long time elapses between periods of reheating due to reflected acoustic waves, whereas in a small cell the reflected waves return more quickly and the initial excitation volume remains generally hotter (cf. refs. 27, 31 and the discussion below). The cell geometry did in fact affect the intensity and character of the visible emission (the less was the intensity, the less was the continuum in the larger cell) and, as indicated below, the distribution of end products from the fuel–SF_6 reactions.

An analysis similar to that presented elsewhere [27] for laser ignition of fuel–oxygen mixtures was used to examine the ignition delay behavior of CO_2-laser-irradiated CH_4–SF_6 mixtures (1:1) as a function of the absorbed laser energy and initial pressure. For the experimental conditions in this study, the time period t_{ig} in which ignition delays could be observed (and distinguished from other sources of luminescence such as window fluorescence) was approximately 3 - 500 μs after the start of the laser pulse. Several factors which could in principle influence the reactions in a system of this type probably occur well outside this period. For example, at pressures of

8 - 50 Torr energy transfer from vibrationally excited SF_6 probably drives the local molecular ensemble to near-statistical equilibrium in a few microseconds (the vibration–translation relaxation time for SF_6 is 150 μs at 1 Torr for $v_3 = 1$ [32]; the relaxation time for highly vibrationally excited SF_6 is probably much smaller [3]). The observed ignition delays, however, are short compared with the time required for ordinary macroscopic heat transport in this experimental design [27]. Pre-ignition reactions presumably supply chemical energy to the system; however, for most combustion reactions [33] the temperature increase during t_{ig} is much smaller than the initial temperature (in this case the temperature achieved by laser heating). Hence, to a first approximation the ignition delay data can be analyzed by calculating the rapidly thermalized energy distribution generated in the sample by the laser pulse and accounting for the effects of hydrodynamic motion on this distribution.

As before [27], the first step in calculating the initial temperature distribution is to give a phenomenological description of the absorption of pulsed CO_2 laser radiation by the CH_4 and SF_6 molecules in the various samples. The dependence of the absorption cross section σ on the laser energy fluence Φ is determined by fitting energy transmission data using numerical techniques [34, 35] incorporating the model beam profile described in Section 2 and a cylindrically symmetric model reaction cell (of equal length and cross-sectional area to the actual test cell). The laser energy fluence incident on the sample is given by [34]

$$\Phi(r, z = 0) = \frac{2E_G'}{\pi^{3/2}(0.73 \text{ cm})^2} \exp\left\{-\left(\frac{r}{0.73 \text{ cm}}\right)^4\right\} \tag{1}$$

where E_G' represents the laser energy passing through the input window of diameter 2.5 cm (see ref. 27 for details of window transmission etc.). The sample absorbs the laser radiation according to the equation

$$\frac{\partial \Phi}{\partial z} = -\Phi(r, z)\,\sigma(\Phi)\rho \tag{2}$$

where ρ is the density of the absorbing gas (i.e. SF_6). The analysis does not include absorption of laser energy reflected from the rear window; however, the error introduced by this simplification is probably fairly small [27]. If an assumed functional form is taken for $\sigma(\Phi)$, successive numerical integrations can be used to obtain $\Phi(r, l)$, where $l = 5$ cm is the cell length, and a calculated fractional energy transmission τ_{calc} given by

$$\tau_{calc} = \frac{1}{E_G}\left\{\int_0^{r_c}\Phi(r, l)2\pi r\, dr\right\} \tag{3}$$

where r_c is the radius of the model reaction cell and E_G is the total energy incident on the sample; E_G is slightly less than E_G' since the cell walls skim about 3% of the energy from the outer part of the beam.

In keeping with the observed power law behavior of multiple-photon absorption in SF_6 alone [35], a simple expression of the form

$$\sigma(\Phi) = \sigma_L \Phi^{-\beta}$$

where σ_L and β are constants proved to be sufficient to describe the IR absorption by the CH_4–SF_6 mixtures. For fixed sample pressure, observed fractional energy transmissions τ were compared with calculated values over the fluence range of interest. The average error ϵ for m data points is given by

$$\epsilon = \frac{1}{m} \sum_{i=1}^{m} \frac{|\tau - \tau_{\text{calc}}|}{\tau} \tag{4}$$

This quantity was minimized by simultaneous variation in the initial $\sigma(\Phi)$ parameters using a simplex optimization technique [36].
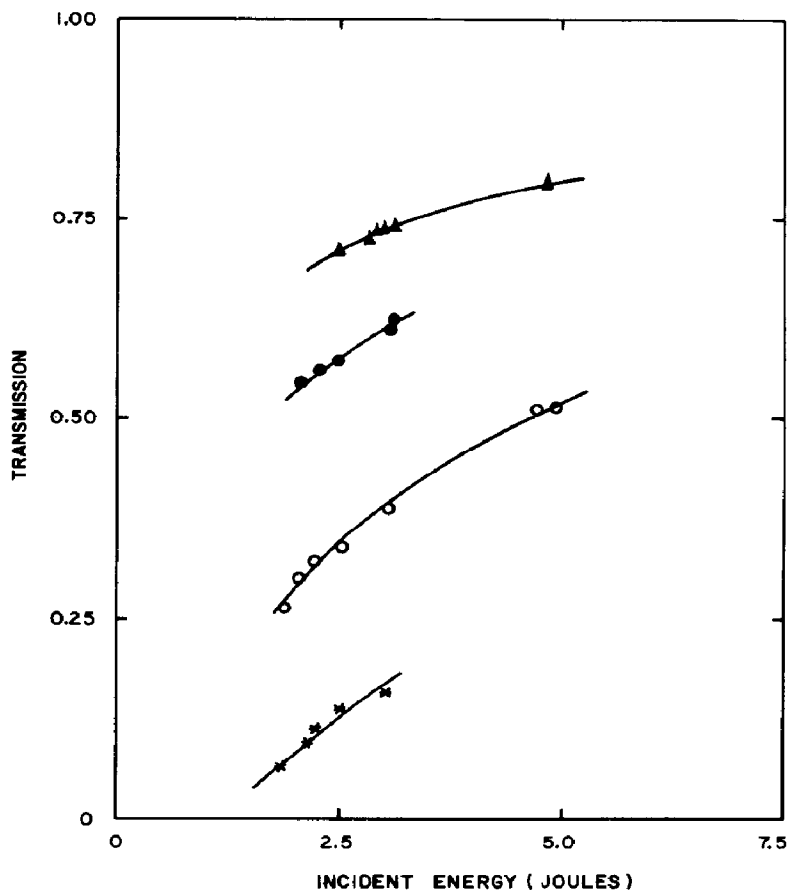

Fig. 3. Numerical fits to observed energy transmission data using the simplex optimization data reduction technique described in the text. The energy transmission is plotted against the total laser energy passing through the input window for a 1:1 mixture of SF_6 and CH_4 at various pressures: ▲, 8 Torr; ●, 12 Torr; ○, 20 Torr; *, 30 Torr.

The numerical fits to observed transmission data are shown in Fig. 3. Mixtures at higher pressures were also examined; however, these samples absorbed the laser radiation so strongly that it was not possible to model the data confidently. Optimized $\sigma(\Phi)$ expressions for the data sets successfully modeled are listed in Table 1 together with derived $\eta(\Phi)$ functions, where η represents the average number of photons absorbed per molecule. The apparent functional relationship $\eta(\Phi) \propto \Phi^\gamma$, where $\gamma \approx 0.45$, is roughly consistent with the observed departure from a simple $\Phi^{2/3}$ dependence for low pressure (0.1 Torr) SF_6 when this gas is mixed with buffer gas at 3 - 100 Torr [37].

TABLE 1

Phenomenological $\sigma(\Phi)$ and $\eta(\Phi)$ relationships for 1:1 mixtures of CH_4 and SF_6

Sample pressure (Torr)	$\sigma(\Phi)$[a] (cm^2)	$\eta(\Phi)$[b]
8	$4.90 \times 10^{-19} \Phi^{-0.56}$	$26.5\Phi^{0.44}$
12	$5.03 \times 10^{-19} \Phi^{-0.545}$	$27.2\Phi^{0.455}$
20	$5.22 \times 10^{-19} \Phi^{-0.57}$	$28.2\Phi^{0.43}$
30	$5.60 \times 10^{-19} \Phi^{-0.53}$	$30.3\Phi^{0.47}$

[a] Molecular absorption cross section.
[b] Average number of photons absorbed per molecule.

If a phenomenological molecular absorption cross section $\sigma(\Phi)$ is assumed and hydrodynamic motion and macroscopic energy transport during the laser pulse are neglected, the energy E deposited in a volume exposed to energy fluence Φ is equal to $\Phi \sigma(\Phi)\rho$. For any input fluence with a functional form given by eqn. (1), a detailed absorption profile in the model sample geometry can be calculated by numerical integration of eqn. (2). The corresponding initial temperature profile $T_i(r, z)$ can be derived using the relation

$$\left(\frac{\partial E}{\partial T}\right)_v = C_v(T) \tag{5}$$

where C_v is the temperature-dependent heat capacity [38] of the sample at constant volume. The effects of hydrodynamic motion on such temperature distributions, as well as on the pressure and density profiles of the irradiated samples, were modeled using a computer code for two-dimensional wave propagation [39]. The samples were described by an equation of state which included the temperature dependence of C_v; however, ordinary heat transport processes and heat generation from chemical reactions were not addressed by the code. More details of problem initialization are given in ref. 27. The complex physical behavior which may be introduced by hydrodynamic motion is illustrated by results for a typical case shown in Fig. 4. According to the code, the sample experiences a significant rarefaction at the
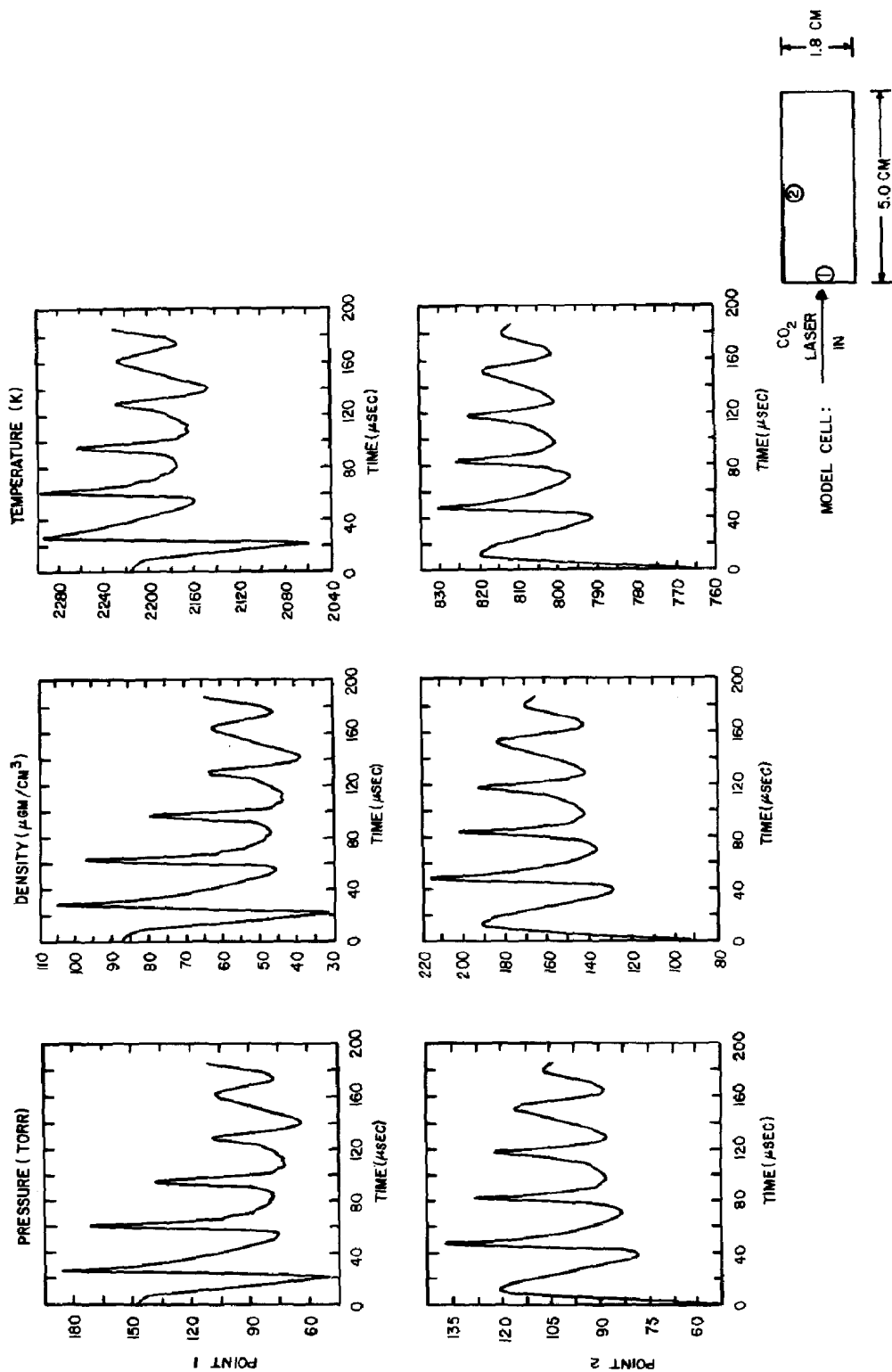
Fig. 4. Pressure–time, density–time and temperature–time histories at two points in the model reaction cell calculated using the TOODY IV wave propagation computer code [39]: point 1, region of maximum energy deposition (also, minimum ignition delay as seen by the PMTs); point 2, sample region adjacent to the piezoelectric pressure transducer. The initial conditions correspond to irradiation of a mixture of CH_4 at 10 Torr and SF_6 at 10 Torr at an incident laser energy of 2.5 J.

center of the cell accompanied by parameter oscillations which can be identified by period and phase relationships as arising from strong radial acoustic waves (weak shocks initially) and much weaker longitudinal waves. The code predictions have been found to be in good agreement with the salient features of pressure histories recorded by a pressure transducer mounted on the side of a cylindrical test cell [27]. As expected, observed pressure histories in the square sample geometry exhibit similar but somewhat more complicated behavior. The fluctuations in pressure, density and temperature are evidently also fairly sensitive to beam alignment relative to the cell axis [40].

Figure 5 shows calculated results for the temperature dependence of ignition delay for various initial pressures of 1:1 mixtures of CH_4 and SF_6. In this figure, observed t_{ig}s were correlated with the average temperatures (during the induction period) in the region of maximum energy deposition as determined by eqns. (2) and (5) and adjusted according to the results of the hydrodynamic simulations. In the experimental configuration used in this study, hydrodynamic motion apparently perturbs the initial temperature distribution much less than the corresponding pressure and density profiles. In fact, Fig. 4 indicates that the time-averaged temperature probably differs
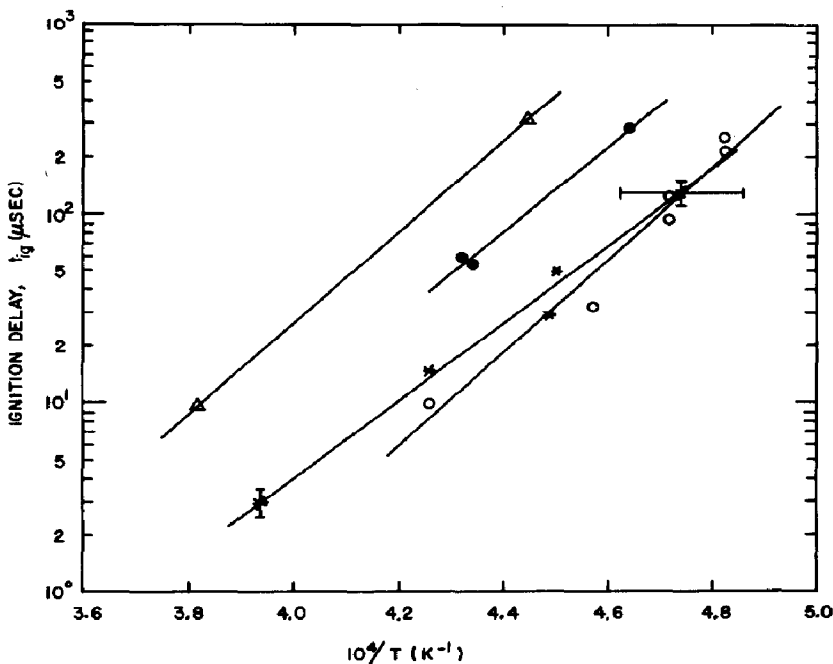

Fig. 5. Semilogarithmic plots of ignition delay $vs.$ T^{-1} for the SF_6–CH_4 mixtures (1:1): △, 8 Torr; ●, 12 Torr; ○, 20 Torr; *, 30 Torr. Least-squares line fits to each data set are included. The vertical error bars shown indicate the typical uncertainty in assigning the ignition delay (*i.e.* the time between the laser pulse and the onset of intense and prolonged luminescence) from the recorded PMT signals. According to the shock code, the temperature of the sample in the region of maximum energy deposition is predicted to lie within the range indicated by the horizontal error bar for more than 90% of the time between the laser pulse and ignition.

from the initial temperature T_i ($r = 0, z = 0$) by no more than a few per cent during ignition delay periods of interest. Within the limitations of the model, the data indicate an approximately linear relationship between $\ln t_{ig}$ and T^{-1}. In addition, the slope appears to be essentially invariant over the 8 - 30 Torr range of initial pressure. As such, the apparent functional form is roughly consistent with the following relationship predicted by thermal explosion theory [41]:

$$\ln t_{ig} \approx \frac{E_{act}}{RT} + B \tag{6}$$

where E_{act} corresponds to an overall activation energy, R is the gas constant and B is a constant. According to eqn. (6) and the slopes in Fig. 5, $E_{act} \approx$ 100 kcal mol^{-1} for the CH$_4$–SF$_6$ system. In the fuel–oxygen ignition study [27], activation energies so derived were generally in good agreement with available data obtained from shock tube and hot air stream injection techniques. Unfortunately, comparable published values apparently do not exist for high temperature hydrocarbon–SF$_6$ reactions. In any case, the analysis presented above is tentative and further work will be required to decide whether or not the thermal explosion theory really provides an adequate description of the laser-initiated CH$_4$–SF$_6$ reactions. It is certainly clear from Fig. 4 that the role of pressure in these reactions is difficult to characterize using the present experimental design; i.e. the pressure does not remain constant during the induction period. The time-averaged gas density in the ignition region may be a more useful parameter in this regard.

Some insight into the chemistry of CO$_2$-laser-initiated fuel–SF$_6$ reactions can be gained by analysis of the IR absorption spectra of post-irradiated samples. Identified end products from selected mixtures are given in Table 2. In all cases substantial quantities of the starting materials were observed, indicating that the reactions normally do not go to completion. Cell geometry apparently has a significant effect in this regard as much lower concentrations of the reactants remained when the reactions were initiated in a small cell. For CH$_4$, CH$_3$OH and CH$_2$F$_2$, stable hydrocarbon intermediates were not seen in the end products. Rather, the occurrence of completely substituted species such as CS$_2$, CF$_4$ and C$_2$F$_4$ strongly suggests that, as intermediates are formed in the laser-initiated reactions, facile hydrogen abstraction takes place. Richer IR absorption spectra were seen for mixtures containing nitromethane, n-propyl nitrate and isopropyl nitrate. In these samples, many compounds normally observed [42, 43] in thermal decomposition of the parent species (e.g. CH$_4$, H$_2$CO and acetaldehyde) appeared as end products; however, these decomposition products may have formed on the cooler periphery of the excitation volume. The common occurrence of HCl, SiF$_4$ and Na$_2$SiF$_6$ is evidence of chemical attack on the quartz cell and NaCl windows.

Many details of these CO$_2$-laser-initiated reactions remain undetermined. From their initial results on low pressure hydrocarbon–SF$_6$ mixtures, Orr and Keentok [13] concluded that the observed luminescent

TABLE 2

Summary of IR absorption spectra of selected fuel–SF_6 mixtures after irradiation by a pulsed CO_2 laser

Reactants	Incident laser energy (J)	End products detected[a]
CH_4–SF_6 (40 Torr; 1:1 mixture; large cell)	4.5	CH_4, SF_6, CS_2, CF_4, C_2F_4, HCl, SiF_4[b]
CH_3OH–SF_6 (50 Torr; 3:2 mixture; small cell)	4.6	CH_3OH, SF_6, CO, OCS, CS_2, HCl, SiF_4
CH_2F_2–SF_6 (20 Torr; 1:1 mixture; large cell)	4.7	CH_2F_2, SF_6, CF_4, C_2F_4, SF_4
CH_3NO_2–SF_6 (35 Torr; 4:3 mixture; large cell)	4.4	CH_3NO_2, SF_6, CH_4, HF, CO, OCS, NO, H_2CO, CS_2, SF_4, HCl, SiF_4[c]
n-propyl nitrate–SF_6 (20 Torr; 1:1 mixture; large cell)	4.5	n-propyl nitrate, SF_6, CH_4, HF, CO, OCS, NO, H_2CO, CS_2, nitroalkanes, SF_4, SiF_4, HCl (?), SiO_2 (?), Na_2SiF_6
Isopropyl nitrate–SF_6 (30 Torr; 1:1 mixture; large cell)	4.5	Isopropyl nitrate, SF_6, CH_4, HF, CO, OCS, NO, CH_3CHO, CS_2 (?), nitroalkanes, NO_2 (?), SiF_4, SF_4, HCl (?), Na_2SiF_6

[a] Tentative identifications are designated by question marks.
[b] Spectrum contained an unidentified absorption band near 2095 cm^{-1}.
[c] Spectrum contained an unidentified absorption feature (doublet) near 1800 cm^{-1}.

hydrocarbon dissociation did not result from a thermal mechanism involving translationally hot gas. They proposed instead a fluorine atom chemistry route to the luminescence by means of SF_6 photodissociation; however, Cantrell et al. [3] subsequently argued that this claim for a deviation from thermal chemistry might be premature. Other reaction schemes appropriate to systems of this type have been discussed by Cox and Kaldor [19] and Bauer and Haberman [30]. Much of the experimental evidence in this study is consistent with reaction initiation via dissociation of SF_6 (thermally or otherwise) to produce fluorine atoms [44, 45] followed by hydrogen abstraction. This evidence includes the similarity of the observed luminescence to that seen in atomic-fluorine-supported flames [29] as well as the difficulty in igniting NH_3 relative to CH_4. With regard to the latter phenomenon, it is known that the rate constant for hydrogen abstraction by fluorine atoms is much smaller for NH_3 than that for CH_4, even though the exothermicities are quite similar [46].

To gain further information on reaction initiation in these systems, qualitative measurements of ease of ignition (i.e. how much incident laser

energy is required at a given mixture ratio and pressure) for CH_4, CH_3F, CH_2F_2 and CHF_3 were compared with known rate constants for abstraction. The rate constants vary according to $k_{CH_4} \approx k_{CH_3F} > k_{CH_2F_2} \gg k_{CHF_3}$ [46]. A similar trend in ease of ignition would be expected if abstraction of the initial hydrogen atom by a fluorine atom were the rate-determining step in each case; however, CH_2F_2 proved to be the most reactive. The easily achieved ignition of CH_2F_2–SF_6 cannot readily be explained by differences in energy absorption or temperature since all of these fuels are such poor absorbers at 10.718 μm that SF_6 dominates the absorption as well as the heat capacity of the various mixtures. Rather, the observed trend is generally consistent with the published results of Pariiskaya and Vedeneev [47 - 50] and Seeger *et al.* [51]. These studies have shown that the fluorination (starting with molecular fluorine) of methane and its fluoroderivatives occurs by chain reactions which proceed over stable intermediate fluoroderivatives to the end product CF_4. Energetic chain branching occurs in the case of CH_2F_2. Consequently this compound is the most reactive in the series and acts as a degenerate branching agent in the fluorination of CH_4 and CH_3F. By comparison the ignition results in this study suggest a prominent role for hydrocarbon fluorination via similar complex chain reactions involving hydrogen abstraction.

The results of CO_2 laser excitation of CH_4–S_2F_{10} mixtures are also interesting in terms of possible reaction mechanisms. The production of flame-like visible luminescence in CH_4–S_2F_{10} samples requires higher incident and absorbed energies than those needed for ignition of comparable CH_4–SF_6 mixtures; however, the increased heat capacity of S_2F_{10} (relative to SF_6) largely compensates for the increased energy deposition such that the initial temperatures achieved in the CH_4–S_2F_{10} samples are almost the same as in those containing SF_6. While fluorine atoms (and SF_5) are readily produced from excited SF_6, S_2F_{10} apparently dissociates primarily into two SF_5 radicals [34]; hence vibrationally or translationally hot SF_5 may play an important role in reactions of this type. In contrast, fluorine atoms may also be important in reactions starting with S_2F_{10} since SF_5 may be further dissociated into SF_4 and F [52]. Finally, ion chemistry may be significant in a complete description of these reactions. According to the Saha relation, 10^{11} - 10^{13} ions cm^{-3} should be present in the excitation volume under typical pressure and temperature conditions. Chemi-ionization kinetics are probably also important [53].

4. Conclusions

CO_2 laser excitation of SF_6–fuel and S_2F_{10}–fuel mixtures has been examined under experimental conditions leading to the initiation of highly luminous reactions. The visible emission produced in the irradiated mixtures is similar in many respects to that observed in molecular-fluorine-supported flames and discharge-initiated atomic-fluorine-supported flames. The time

delay to ignition in these mixtures is a readily observable function of absorbed laser energy. In the case of SF_6–CH_4 mixtures the laser-generated temperature, pressure and density conditions resulting in ignition have been calculated by means of an analysis that includes a phenomenological description of fluence-dependent absorption in the samples and modeling of subsequent hydrodynamic effects during the induction period. The end product analysis of post-irradiated SF_6–hydrocarbon samples points to efficient routes for hydrogen abstraction leading to completely substituted species such as CS_2, CF_4 and C_2F_4. Ignition studies on mixtures of SF_6 with CH_4 and its fluoro derivatives indicate that CH_2F_2 is the most reactive species in the series, in agreement with previous fluorination experiments on these compounds. In view of the probable complexity of the laser-initiated reactions, full characterization of the chemistry in these systems will undoubtedly require studies utilizing appropriate real-time (*e.g.* laser spectroscopic) probes of the kinetics.

Acknowledgments

References

1 J. P. Aldridge, J. H. Birely, C. D. Cantrell and D. C. Cartwright, *Phys. Quantum Electron.*, *4* (1976) 57.
2 R. V. Ambartzumian and V. S. Letokhov, in C. B. Moore (ed.), *Chemical and Biochemical Applications of Lasers*, Vol. 3, Academic Press, New York, 1977, p. 167.
3 C. D. Cantrell, S. M. Freund and J. L. Lyman, in M. L. Stitch (ed.), *Laser Handbook*, Vol. 3, North-Holland, Amsterdam, 1979, p. 485.
4 R. T. Bailey and F. R. Cruickshank, *Annu. Rep. Prog. Chem., Sect. A, 75* (1979) 49.
5 P. A. Schulz, Aa. S. Sudbø, D. J. Krajnovich, H. S. Kwok, Y. R. Shen and Y. T. Lee, *Annu. Rev. Phys. Chem., 30* (1979) 379.
6 R. G. Harrison and S. R. Butcher, *Contemp. Phys.,* 21 (1980) 19.
7 S. H. Bauer, E. Bar-Ziv and J. A. Haberman, *IEEE J. Quantum Electron., 14* (1978) 237.
8 R. A. Hill and G. A. Laguna, *Opt. Commun., 32* (1980) 435.
9 R. A. Hill, *Appl. Opt., 20* (1981) 2239.
10 E. Würzberg, A. J. Grimley and P. L. Houston, *Chem. Phys. Lett., 57* (1978) 373.
11 E. Würzberg and P. L. Houston, *J. Chem. Phys., 72* (1980) 4811.
12 E. Würzberg and P. L. Houston, *J. Chem. Phys., 72* (1980) 5915.
13 B. J. Orr and M. V. Keentok, *Chem. Phys. Lett., 41* (1976) 68.
14 M. Rothschild, W. S. Tsay and D. O. Ham, *Opt. Commun., 24* (1978) 327.
15 M. Rothschild, W. S. Tsay and D. O. Ham, *J. Opt. Soc. Am., 68* (1978) 683.
16 G. F. Nutt and B. J. Orr, *Opt. Commun., 29* (1979) 57.
17 C. R. Quick, Jr., and C. Wittig, *Chem. Phys. Lett., 48* (1977) 420.

18 J. M. Preses, R. E. Weston, Jr., and G. W. Flynn, *Chem. Phys. Lett.*, *48* (1977) 425.
19 D. M. Cox and A. Kaldor, *Opt. Commun.*, *31* (1979) 153.
20 J. L. Lyman and R. J. Jensen, *J. Phys. Chem.*, *77* (1973) 883.
21 N. N. Akinfiev, N. G. Basov, V. T. Gelochkin, S. I. Zavorotnyi, E. P. Markin, A. N. Oraevskii and A. V. Pankratov, *JETP Lett.*, *19* (1974) 383.
22 V. I. Balykin, Yu. R. Kolomiiskii and O. A. Tumanov, *Sov. J. Quantum Electron.*, *5* (1975) 454.
23 A. V. Belotserkovets, G. A. Kirillov, S. B. Kormer, G. G. Kochemasov, Yu. V. Kuratov, V. I. Mashendzhinov, Yu. V. Savin, E. A. Stankiev and V. D. Urlin, *Sov. J. Quantum Electron.*, *5* (1975) 1313.
24 V. T. Galochkin, S. I. Zavorotnyi, V. N. Kosinov, A. A. Ovchinnikov, A. N. Oraevskii and N. F. Starodubtsev, *Sov. J. Quantum Electron.*, *6* (1976) 66.
25 N. G. Basov, V. T. Galochkin, V. G. Kartyshov, A. G. Lyapin, I. M. Mazurin, A. N. Oraevskii and N. F. Starodubtsev, *Sov. Phys. — JETP*, *45* (1977) 479.
26 J. C. Cummings, *Opt. Commun.*, *35* (1980) 399.
27 W. M. Trott, *J. Appl. Phys.*, *54* (1983) 118.
28 R. A. Durie, *Proc. R. Soc. London, Ser. A*, *211* (1952) 110.
29 G. Schatz and M. Kaufman, *J. Phys. Chem.*, *76* (1972) 3586.
30 S. H. Bauer and J. A. Haberman, *IEEE J. Quantum Electron.*, *14* (1978) 233.
31 D. F. McMillen, K. E. Lewis, G. P. Smith and D. M. Golden, *J. Phys. Chem.*, *86* (1982) 709.
32 R. D. Bates, J. T. Knudtson, G. W. Flynn and A. M. Ronn, *J. Chem. Phys.*, *57* (1972) 4174.
33 N. N. Semenov, *Chemical Kinetics and Chain Reactions*, Clarendon, Oxford, 1935.
34 J. L. Lyman and K. M. Leary, *J. Chem. Phys.*, *69* (1978) 1858.
35 J. L. Lyman, R. G. Anderson, R. A. Fisher and B. J. Feldman, *Chem. Phys.*, *45* (1980) 325.
36 D. E. Long, *Anal. Chim. Acta*, *46* (1969) 193.
37 O. P. Judd, *J. Chem. Phys.*, *71* (1979) 4515.
38 D. R. Stull and H. Prophet (eds.), JANAF thermochemical tables, 2nd edn., *NBS Natl. Stand. Ref. Data Ser. 37*, June 1971 (National Bureau of Standards, U.S. Department of Commerce).
39 J. W. Swegle, TOODY IV — a computer program for two-dimensional wave propagation, *Rep. SAND78-0552*, September 1978 (Sandia National Laboratories, Albuquerque, NM).
40 G. P. Smith and R. M. Laine, *J. Phys. Chem.*, *85* (1981) 1620.
41 R. S. Brokaw, Thermal ignition, with particular reference to high temperatures. In M. W. Thring (ed.), *Selected Combustion Problems, Proc. 2nd Agard Colloq.*, Butterworths, London, 1956, pp. 115 - 138.
42 J. Powling and W. A. W. Smith, *Combust. Flame*, *1* (1957) 308.
43 P. Beeley, J. F. Griffiths and P. Gray, *Combust. Flame*, *39* (1980) 269.
44 R. L. Wilkins, *J. Chem. Phys.*, *51* (1969) 853.
45 M. J. Coggiola, P. A. Schulz, Y. T. Lee and Y. R. Shen, *Phys. Rev. Lett.*, *38* (1977) 17.
46 T. L. Pollock and W. E. Jones, *Can. J. Chem.*, *51* (1973) 2041.
47 V. I. Vedeneev and A. V. Pariiskaya, *Kinet. Catal.*, *12* (1971) 14.
48 A. V. Pariiskaya and V. I. Vedeneev, *Kinet. Catal.*, *12* (1971) 252.
49 A. V. Pariiskaya and V. I. Vedeneev, *Kinet. Catal.*, *12* (1971) 481.
50 A. V. Pariiskaya and V. I. Vedeneev, *Kinet. Catal.*, *12* (1971) 750.
51 C. Seeger, G. Rotzoll, A. Lübbert and K. Schügerl, *Int. J. Chem. Kinet.*, *14* (1982) 457.
52 E. R. Grant, M. J. Coggiola, Y. T. Lee, P. A. Schulz, Aa. S. Sudbø and Y. R. Shen, *Chem. Phys. Lett.*, *52* (1977) 595.
53 F. F. Crim, G. H. Kwei and J. L. Kinsey, *Chem. Phys. Lett.*, *49* (1977) 526.